Dual focus polarisation splitting lens

PAUL MOSELEY,[1,*] **GIORGIO SAVINI,**[2] **JIN ZHANG,**[3] **AND PETER ADE**[1]

[1]*School of Physics and Astronomy, Cardiff University, The Parade, CF24 3AA Cardiff, Wales, UK*
[2]*Optical Science Laboratory, Physics and Astronomy Department, University College London, Gower Street, London WC1E 6BT, UK*
[3]*Department of Computing and Technology, Faculty of Science and Technology, Anglia Ruskin University, Compass House, 80 Newmarket Road, Cambridge, CB5 8DZ, UK*
*paul.moseley@astro.cf.ac.uk

Abstract: We have successfully designed and measured a unique polarisation splitting lens which focuses the orthogonal linear polarisations side-by-side in the lens focal plane. This concept can find application in situations where there is limited space for the beam splitters and focusing optics that are required for incoherent detectors.

References and links

1. G. Savini, P. A. R. Ade, and J. Zhang, "A new artificial material approach for flat THz frequency lenses," Opt. Express **20**(23), 25766–25773 (2012).
2. G. Pisano, M. W. Ng, F. Ozturk, B. Maffei, and V. Haynes, "Dielectrically embedded flat mesh lens for millimeter waves applications," Appl. Opt. **52**(11), 2218–2225 (2013).
3. N. Yu and F. Capasso, "Flat optics with designer metasurfaces," Nat. Mater. **13**(2), 139–150 (2014).
4. N. Marcuvitz, *Electrical Engineers, Waveguide Handbook* (McGraw-Hill, 1951).
5. R. Ulrich, "Far-infrared properties of metallic mesh and its complementary structure," Infrared Phys. **7**(1), 37–55 (1967).
6. S.-W. Lee, G. Zarrillo, and C.-L. Law, "Simple formulas for transmission through periodic metal grids or plates," IEEE Trans. Antenn. Propag. **30**(5), 904–909 (1982).
7. J. Zhang, P. A. R. Ade, P. Mauskopf, L. Moncelsi, G. Savini, and N. Whitehouse, "New artificial dielectric metamaterial and its application as a terahertz antireflection coating," Appl. Opt. **48**(35), 6635–6642 (2009).
8. T. Timusk and P. L. Richards, "Near millimeter wave bandpass filters," Appl. Opt. **20**(8), 1355–1360 (1981).
9. G. Zarrillo and K. Aguiar, "Closed-form low frequency solutions for electromagnetic waves through a frequency selective surface," IEEE Trans. Antenn. Propag. **35**(12), 1406–1417 (1987).
10. J. B. Caldwell, "Optical design with Wood lenses 1: infinite conjugate systems," Appl. Opt. **31**(13), 2317–2325 (1992).
11. P. Ade, G. Pisano, C. Tucker, and S. Weaver, "A review of metal mesh filters," in Society of Photo-Optical Instrumentation Engineers (SPIE) Conference Series, (2006).
12. D. H. Martin and E. Puplett, "Polarised interferometric spectrometry for the millimetre and submillimetre spectrum," Infrared Phys. **10**(2), 105–109 (1970).
13. M. D. Niemack, P. A. R. Ade, J. Aguirre, F. Barrientos, J. A. Beall, J. R. Bond, J. Britton et al. "ACTPol: a polarization-sensitive receiver for the Atacama Cosmology Telescope," *https://arXiv:1006.5049* (2010).

1. Introduction

It has been recently shown that metal mesh technology can be used to create a flat lenses [1–3]. In general, these types of lens offer a viable alternative to traditional dielectric counterparts with the advantage of having reduced thickness and hence mass for a lens of comparable focal length. Metamaterial lenses can be divided into two classes; those using a periodic structure to provide a variable phase [2,3] across the aperture and those using a stack of meshes [1] to vary the refractive properties of the material. The phase approach can be used as single surfaces as outlined in the review by Yu et al. [3] or as stacks of phased surfaces as demonstrated by Pisano [2]. An issue with the phase approach is that the chosen unit cell design has to be able to generate the entire required phase change, which usually leads to a design that is resonant, thus narrow band, and has un-wanted polarisation effects. In

contrast, Savini's approach was to use a stack of meshes with radially varying geometry to create a graded-index material that mimics the behaviour of dielectric lenses used at THz frequencies. The attractive property of this design is that the material refractive properties are constant over a broad frequency range rather than being tuned for a particular band.

In this paper we extend the Savini design by exploiting the more exotic properties of the metal mesh structures, with the aim of producing a lens which spatially separates the two orthogonal polarisation states by imaging them side-by-side on the same focal plane. To avoid confusion with the existing flat lenses, we referrer to this new device as a pol-lens.

The advantage of such a device is that two polarisation-insensitive detectors could be placed adjacently in the focal plane to directly measure the linear polarisation state of the incoming beam. Currently, to determine the state of polarisation, beam splitters and polarizers must be used, which open additional ports in a system and enlarge the overall volume of the detecting system. This novel device could thus offer a compact polarimetric detecting unit.

2. Theory and modeling

The lens described by Savini et al. was achieved by adopting a periodic square mesh structure with a given size unit cell which is much smaller ($L \leq \lambda/5$) than the smallest wavelength of interest [1]. The desired operation of the lens was based on the principle that an incoming wave can see a refractive index which decreases radially from its centre which is achieved by making the metalized squares smaller within a fixed periodicity for the mesh. The analytical link between the capacitive nature of such a structure and its geometry has been detailed accurately in [4–6] whilst its relation in close packed form to an equivalent refractive index material is detailed in Zhang (2009) [7] where the manufacture of an artificial dielectric is described.

The design of the pol-lens is based on the same principle except that we now introduce rectangular elements which modify the refractive index along the orthogonal axes. Thus, an incoming wave can now see two distinct refractive indices depending on its linear polarisation state, similar to that of a birefringent crystal. Furthermore, the dependencies of the refractive indices on mesh geometry can be analytically modelled relatively accurately by the use of two parameters; the cell periodicity, g_x or g_y, and the size of the metalized surface within the cell, (g_x-$2a_x$) or, (g_y-$2a_y$) as shown in Fig. 1a along each axis. The polarisation dependencies, as described in [7], can thus be transformed in a spin-like quantity (i.e. a refractive index for each polarisation axis of Fig. 1a). This gives four independent variables that can control the transmission properties of the mesh across the lens surface.

To reduce complexity in the lens design, the outer unit cell size is kept constant ($g = g_x = g_y$) and square. This makes placing the elements for the final design simpler. Furthermore, fine tuning of the effective refractive index of a stack of meshes is controlled by the number of meshes and their spacing (as in Zhang, 2009 [7]) and is used to reduce the complexity of a design for manufacture. Thus, in this design the geometry of the rectangular patches and the ratios (a_x/g) and (a_y/g) control the effective orthogonal refractive indices across the lens similar to a spin quantity.

To design a lens with a specific focal length and diameter, the design parameters are its thickness (number of layers), and its radial geometry profile as specified by the ratios (a_x/g) and (a_y/g), which determine the radial refractive indices.
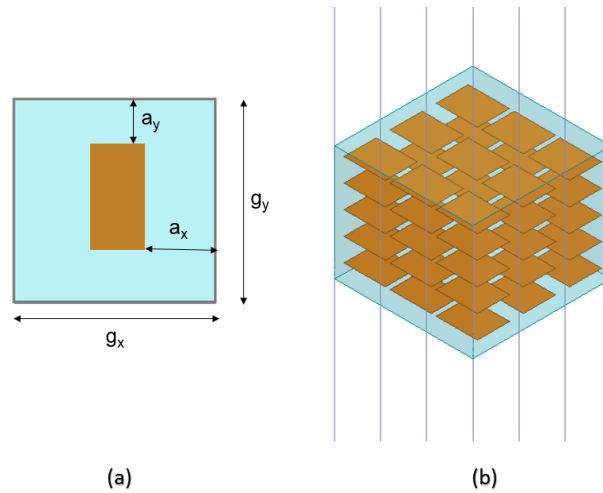
Fig. 1. a) The rectangular unit cell used for designing the pol-lens. b) Example of complete artificial dielectric mesh stack.

2.1 Modelling parameters

Previous work (Zhang, 2009) has shown that the effective refractive index is achieved with only five mesh layers [7]. To reduce the computational time, a single unit cell stack of this minimal structure, as shown in Fig. 1, was modelled in HFSS to verify the polarisation sensitivity of a rectangular patch. Figure 2 shows the transmission of this artificial dielectric for orthogonal linearly polarised waves (x and y). It can be seen that there are two different Fabry-Pérot resonances, thus two different effective indices. For comparison, the fringe pattern expected for a material with uniform refractive index is shown by the dashed curves respectively. The overlap is good for frequencies below 250 GHz and demonstrates that broadband response is achievable. There is also no evidence of cross polarisation occurring in the structure, which is a requirement for the lens.
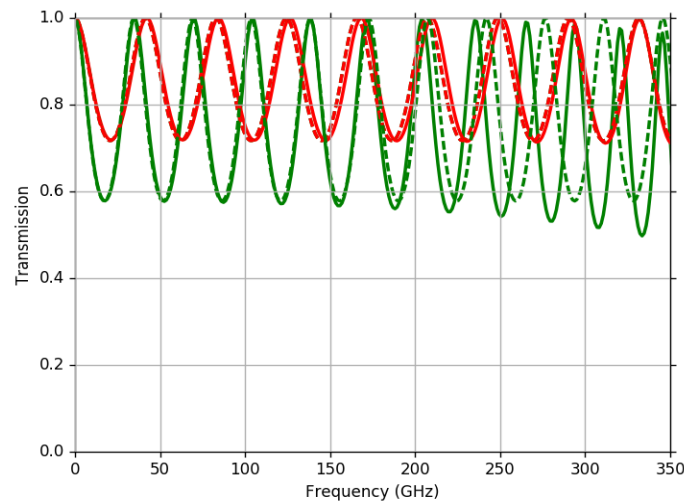

Fig. 2. Typical spectral response of the structure in Fig. 1. g = 200 μm, spacing = 100 μm, a_x/g = 0.05, a_y/g = 0.35. The red curve corresponds to x Polarisation and the green is y polarisation. For comparison, the fringe pattern expected for a material with uniform refractive index is shown by the dashed curves respectively.

Interestingly, the orthogonal nature of the refractive index variations leads to a unique situation in which we can modify the lens's behaviour for linearly polarised inputs which leads to the possibility of changing their respective focal lengths. Alternately, we also perceived that the radial variation of the patch geometry could be designed such that there is a displacement of the lens centre for orthogonal polarisations and hence obtain two focal points which appear side-by-side on the focal plane. We chose the latter design to prototype since it has interesting practical applications.

To design the complete lens, a large array of rectangular patches which vary in size radially is required. The computing time to do this in HFSS was prohibitive so a quicker and hence less accurate model was devised using transmission line (TL) formalism. For this approach, the mesh is represented by an inductive impedance which is related to the mesh geometry as input to an equivalent circuit model.

Previously, for the case of a square patch, we used known impedance relationships [5,6,8]. Since we now require solutions for rectangular patches we used the approach of Zarrillo et al. which is capable of modelling a rectangular patch [9]. Unfortunately, this model does not provide good accuracy but it is able to show the approximate variation of refractive index with geometry and proved sufficient for our demonstration. Further work is needed to find a better equivalent circuit representation.

The design of rectangular mesh stack is chosen such that the effective index is constant over the frequency band of interest, as shown in Fig. 2. However, due to the capacitive nature of the structure used it will reach a cut-off frequency. As this cut-off frequency approaches, the structure starts to change in a way that is similar to a dispersive material, which is that the refractive index increases with frequency as seen in the HFSS model in Fig. 2. This behaviour was seen in the original graded index lens which caused the focal length of the lens to slightly change. For the rectangular patch, there are two different refractive index profiles associated with each side of the rectangle, with each index profile having a different frequency cut off. To address this a rectangular stack representative of a patch used at the centre of the lens has been simulated using the TL code for both orthogonal polarisations. As is evident in Fig. 2, both polarisations have only a slight variation in the Fabry–Pérot fringes when compared to an ideal material of the same index. As the frequency increases, the Fabry–Pérot fringes tail off which is equivalent to an increase in effective refractive index. What is important to note is that both the rate of change in index and the cut-off frequency are different for each polarisation. This means that for higher frequencies the graded index profiles will change slightly which could affect the overall performance of the lens. Although the lens is inherently broadband, its usage should be limited to frequencies below a threshold where the refractive index deviation is non-negligible.

2.2 Exploring the parameter space

The parameter space is explored by using the TL method to determine the refractive index variations for a particular geometry of rectangular patch. This was performed using the existing TL matrix approach to model the behaviour of a stack of 20 meshes, with 100 µm spacing and a cell size of 200 µm. The calculated effective refractive index values for a given incident polarisation as a function of parameters (a_x/g) and (a_y/g) is shown in Fig. 3.
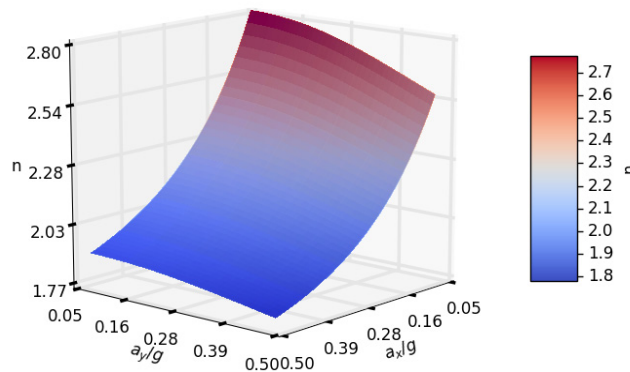
Fig. 3. Parameter space of available refractive index values for one polarisation.

An important conclusion from Fig. 3 is that the refractive index at a specific point on the lens is dependent on both the values of (a_x/g) and (a_y/g) and although there are many possible combinations which fulfil a specific requirement, once chosen there will be a limitation in range for the orthogonal axis. A contour plot of the same data, Fig. 4a, identifies the *parameter pairs* that give rise to a specific refractive index value for one polarisation. The black line highlights selected pairs which give a refractive index of $n = 2.5$ for this polarisation. With the refractive index of this axis fixed Fig. 4b then shows the corresponding range of index values which are available to the orthogonal polarisation as we move incrementally along the black line (for the plot we use a_x/g as a reference for position on the line). This relationship is fundamental to the lens design process.
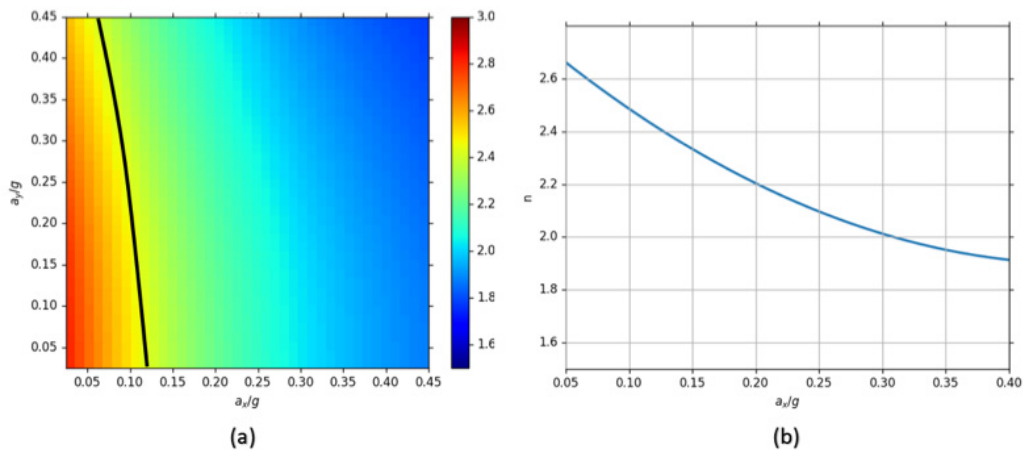

Fig. 4. a) The black line represents the combinations of $(a/g)_x$ and $(a/g)_y$ that lead to a constant index. b) The line shows the range of index vales that are possible for the orthogonal polarisation with same pairs of values.

HFSS was used to test the accuracy of the TL model by using a coarse parameter-space map to limit the computational time. Figure 5 shows the comparison between the two models. The HFSS plot has been interpolated from the original data points and shows that TL model does follow a similar surface profile. This similarity means that the TL model can be used for iterating on an initial design before using HFSS parameter space to populate the final pol-lens design.
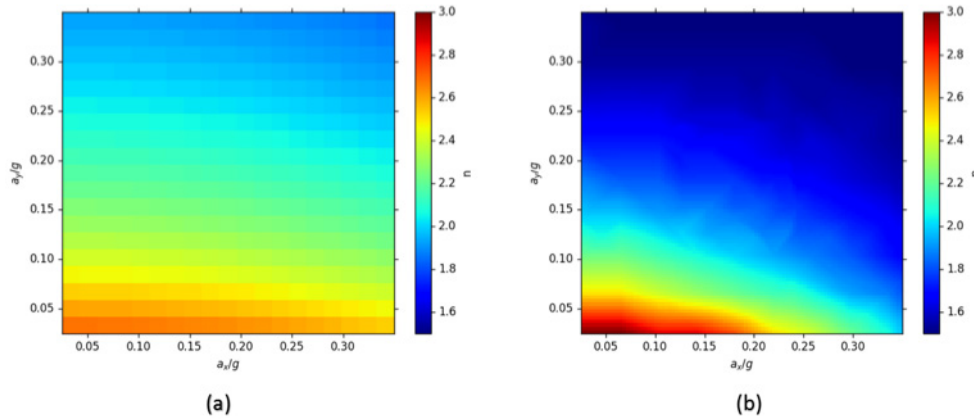
Fig. 5. a) Parameter space realized using a TL b) Interpolated parameter space from HFSS simulations.

3. Lens design and fabrication

The refractive index radial profile, $n(r)$, used for a Woods-type flat lens [10] is given by Eq. (1) where n_0 is the maximum value of n at the lens centre, r is the radial distance from the centre, d is the thickness of the lens and f is its focal length. As discussed in section 2.1, we chose to manufacture a prototype with a displacement of the lens centres for orthogonal polarisations and hence obtain two focal points which appear side-by-side on the focal plane about its central symmetry axis. To minimize the number of unknown variations in this design, the two gradient index (GrIn) profiles for each lens are designed similarly to [1] to have a common focal length of 25 cm, a diameter of 7 cm, and a thickness of 2 mm.

$$n(r) = n_0 - \frac{r^2}{2df}. \tag{1}$$

The overall refractive index distribution of the complete lens is be constructed around a common reference frame. At each point in this reference frame a vector, **n**, is defined which can take two values $\mathbf{n}_x$ and $\mathbf{n}_y$ corresponding the refractive index that each polarisation will see at that point.
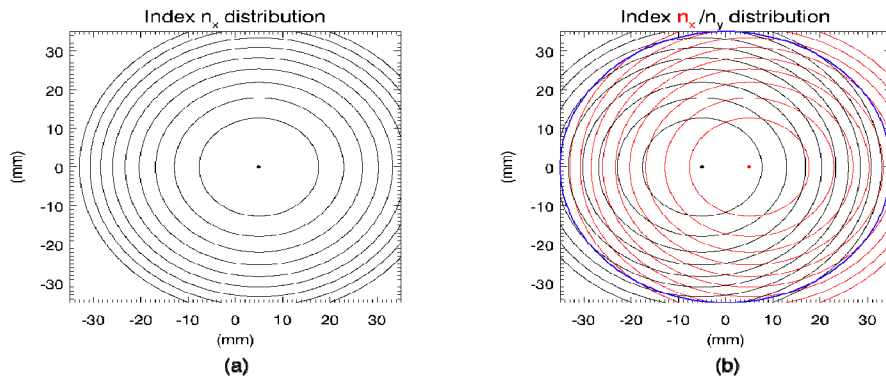

Fig. 6. a) Radial distribution of refractive index for one polarisation. b) The combined refractive index distributions for both polarisations. The physical device boundary is highlighted in blue.

Since each lens has a radially-varying index, there are lines of constant index which form concentric circles around the centre of the lens as shown in Fig. 6a. When the two refractive index profiles are overlapped, as shown in Fig. 6b, the circle of constant index for one polarisation intersects the constant index circles for the other polarisation. The polarisation image separation in the focal plane is simply determined by the separation of the orthogonal polarisation centres. In practice the maximum image separation is partly determined by the range of refractive index as given in Fig. 4b and by the required external diameter.

With the refractive index distribution for the lens defined, it is now possible to use these to determine the mesh geometry (g, a/g) and mesh layer spacing to design the lens. The results of this comparison are shown in Fig. 7. This design is for a lens with a polarised image separation of 10 mm and shows the corresponding values of a/g that produce the required refractive index profiles and thus confirms that manufacture of the lens is viable.
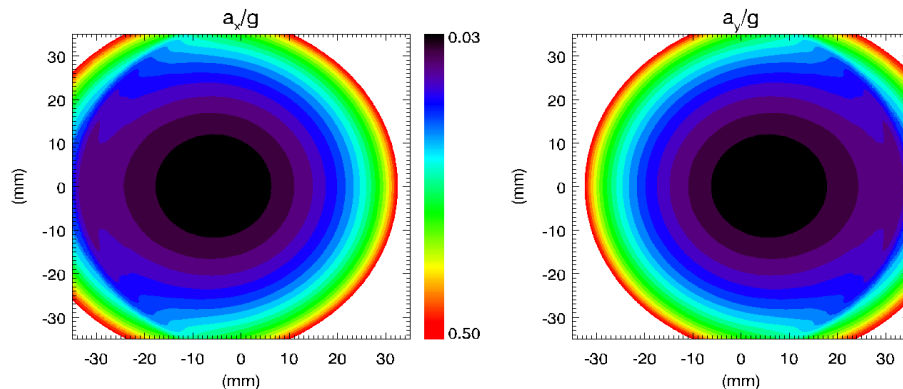

Fig. 7. Maps showing the spatial variation in a/g over the area of the lens for each axis.

One limitation to this design is that any area where the effective index of one GrIn lens falls below that of the substrate (effectively mimicking the flat ring-like slab surrounding a classical convex or planar-convex lens) will not allow for any GrIn behaviour of the other lens, thus breaking the overall cylindrical symmetry of the device at its perimeter. Future studies will investigate potential aberrations, if any, that are induced because of this.

This design was fabricated by hot pressing the mesh layers together with appropriate polypropylene spacers between them as described in Ade & Zhang et al. [7,11]. Only a single mask is required since all the mesh layers are identical; the polarisation asymmetry resides in the distribution profile of the rectangular patches. Like the previous un-polarized design, the lens has not been impedance matched to free space, meaning that there will be reflection losses. This could be addressed by using an anti-reflection coating (ARC) on the surface of the lens. However, since the purpose of this prototype is to test the basic polarisation properties, ARC was not applied.

Care was taken in assembling the pol-lens to ensure that there was minimal rotational misalignment between the meshes as this could introduce unwanted cross-polarisation terms. The completed pol-lens is shown in Fig. 8 with a portion of the mesh pattern highlighted.
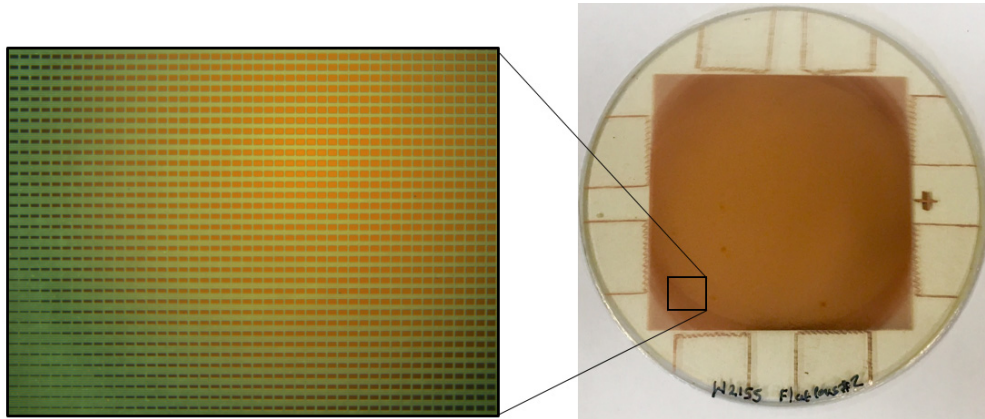
Fig. 8. Image of the pol-lens as built with a zoomed in portion shown.

4. Measurements

4.1 Experimental configuration

The primary goal of the measurement was to validate the lens properties by observing a shift in the focus positon when changing between the orthogonal linear polarisation states. In addition, we also wanted to confirm that the lens was achromatic over a broad spectral range.

To combine both of these measurement requirements we used a Martin-Puplett Fourier Transform Spectrometer (FTS) [12], to provide a polarised radiant source. For our experiment, the output optics of the FTS was coupled to a bolometric detector via a collimating and re-condensing lens system which generates a parallel beam section as shown in Fig. 9. This was convenient because it allowed for a simple spectral and spatial comparisons to be made between a standard polyethylene (PE) lens used as the final condensing optic in this system and the pol-lens by swapping between them. It also ensures that the lens is tested with a collimated input allowing its focal length (distance between lens and detector) to be determined. Differences between the focal length of the PE and pol-lenses where taken into account by re-focusing the detector along the optical axis. Spatial cuts across the focused beams were made by moving the detector orthogonally to the optic axis using a translation stage.

Care was taken to ensure that the pol-lens was aligned such that the optical axis passes through its symmetry centre such that the orthogonal polarisation foci lie on either side of this axis, whilst the PE lens at the same position will focus on axis. This configuration has the advantage that the same amount of power is constantly incident on the lens for both polarisations and both lens types. To measure the lens profiles the detector was mounted on a translation stage which stepped it along the y-axis (see Fig. 9) across the optical axis at the nominal focus position. A full interferometric scan of the FTS was taken at each detector position as it was incremented along the y axis. Thus we can extract transverse beam cuts for any frequency in the spectral range measured (100 – 300 GHz) for either polarisation. The output polarisation state can be selected by rotating the final polarising analyser in the FTS.
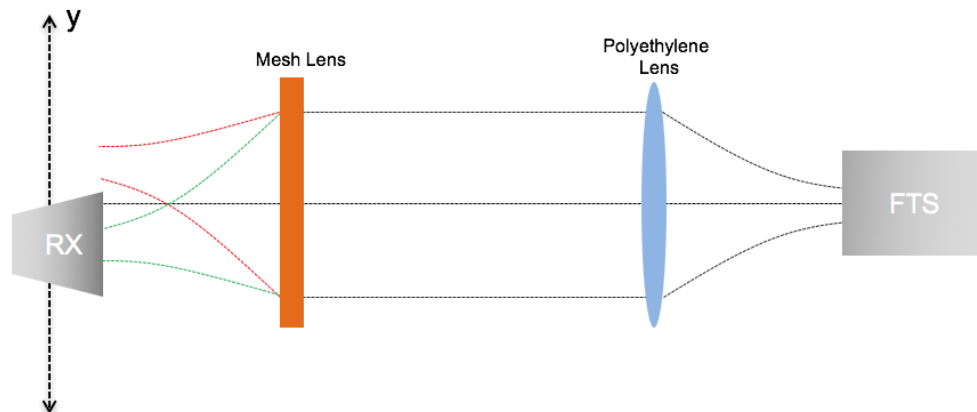
Fig. 9. Experimental setup for measuring the spectral spatial response of the Pol-lens. The output PE lens in a re-imaging telescope at the output of a FT spectrometer is replaced by the pol-lens for comparative measurements. Beam cuts through the final focus are made by scanning the detector transversely across the beam.

An initial reference measurement was taken using the PE lens with the output polarisation orthogonal to the optical bench (S-pol). Full spectral scans (3 GHz resolution) were recorded at each detector position as it was moved ± 50 mm around the optical axis in 1 mm steps. The pol-lens was then inserted and the same scan range repeated. Without any changes in alignment, the output polarisation of the FTS was rotated so that it was perpendicular to the bench (P-pol) and the measurement repeated. Finally, the PE lens was re-inserted and another reference scan taken for the orthogonal polarisation as a systematic check.

4.2 Measured performance

A sequence of scans at different focal positions showed that the optimal focal length of the pol-lens was 230 mm, which is slightly less than the TL design one of 250 mm. A comparison of the orthogonal polarised beam profiles taken at this optimum focus are given in Fig. 10. The data here were normalised for comparison. It can be seen that from fitting the data the focus separation is 8.2 mm, again slightly less than the 10 mm design width.

Because the pol-lens has a longer focal length than the PE lens, its diffraction limited spot size is larger at the detector which has a fixed aperture diameter.
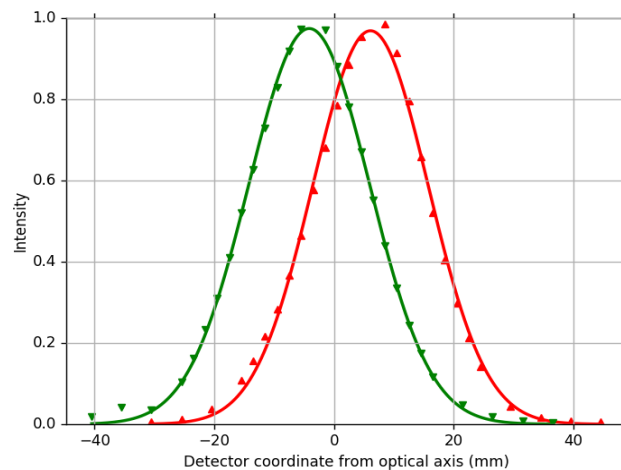

Fig. 10. Cross section of beam profiles for both polarisations at 150 GHz. Vertical polarisation red curve, Horizontal polarisation green curve.

In Fig. 11 we have shifted and overlaid the measured orthogonal beam cuts for the pol-lens to show the symmetry between the polarised outputs. We have also over plotted data from the PE lens and added the diffraction modelling expectations for the measured profiles of both lenses to show the good agreement with expectation. The beam widths of the PE lens and the pol-lens are entirely explained by their different focal lengths (175 mm compared to 230 mm).
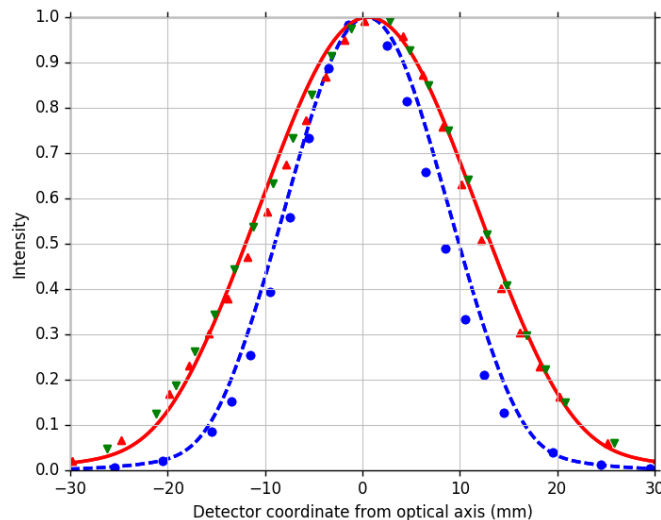

Fig. 11. The orthogonal beam scans at 200 GHz are shifted and overlaid to show the symmetry between the polarisations outputs. Vertical polarisation is red triangles, Horizontal are green inverted triangles. The profile of the polyethylene lens used as a reference is also shown in blue circles. In addition the diffraction model beam cuts are given for the pol-lens red curve and for the PE lens blue dashed curve.

The good agreement between the symmetry for the orthogonal components and the diffraction model is important for practical applications of the lens. Major differences between polarisations would introduce extra systematic errors into a polarimetric measurement whilst departure from the Airy profile would indicate significant issues with the lens form.

The simple diffraction model also allows a comparison of the detected power between the PE and pol-lens as a function of frequency. The beam patterns for each lens, as seen in the detector focal plane, are integrated over the detector aperture to determine the power coupling. By taking the ratio of these as a function of frequency we can remove unknown factors in the source emittance and spectral throughput of the FTS and determine a direct comparison between the lens types as shown in Fig. 12. We have over plotted the measured intensity ratio for the pol-lens/PE lens to show that the spectral behaviour follows the model expectation but is reduced in magnitude at all frequencies. The difference in magnitude seen here is an indication of the excess reflection loss of the pol-lens which is expected because of its higher refractive index over its central area. The difference is surprisingly small, ~9%, which we attribute to the fact that most of its area has an index close to that of PP ($n = 1.48$) which is slightly lower than that of PE ($n = 1.52$) at these wavelengths. Future iteration of the pol-lens will be anti-reflection coated which is relatively easy to implement on the flat lens surfaces with mesh technology.
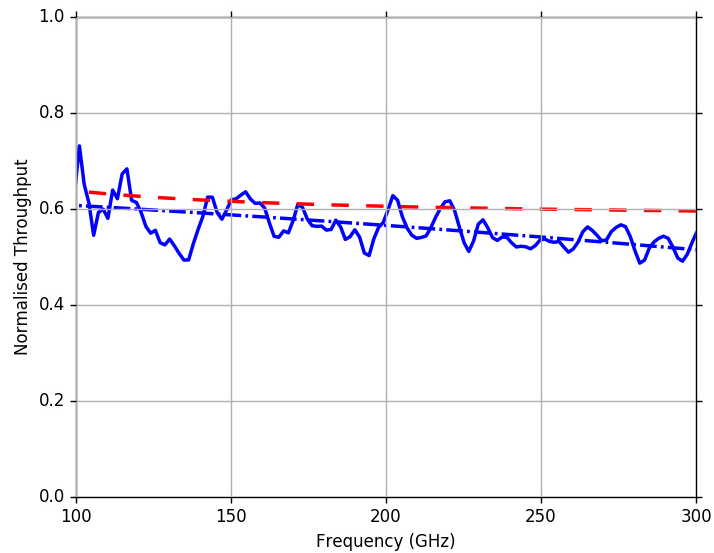
Fig. 12. Comparison of measured on-axis intensity ratio pol-lens/PE lens (blue curve, with a best fit given by blue dash-dotted curve) and the diffraction model power calculations (red dash curve).

5. Conclusion

We designed a novel polarisation splitting lens which is capable of separating the orthogonal linear polarisations and imaging them side by side in its focal plane. This lens thus combines the action of a Wollaston prism and a pair of lenses in a single 2-mm-thick device and is ideal for usage in mm-wave receivers. The measured results show that the prototype lens performs close to expectation over a broad band from 100 to 300 GHz. These results also demonstrate that rectangular meshed patches can be used to separate and steer orthogonal polarisations over a broad frequency range which will assist in the design of other polarisation sensitive meta-material devices.

The size and frequency coverage of the lens demonstrated here was chosen for practical reasons. Future investigation is needed to explore the polarisation separation achievable and the improvement in efficiency achievable with the addition of anti-reflection coated layers. The mesh filter technology has been proven for diameters up to 30 cm allowing usage for a range of applications where large refracting optics are required [13].

Funding